Gd^{3+} Spin–Phonon Interactions in Rare-Earth Fluoride Crystals

M.L. Paradowski* and L.E. Misiak

Institute of Physics, Marie Curie-Skłodowska University
pl. M. Curie-Skłodowskiej 1, 20-031 Lublin, Poland

(Received April 19, 2002)

The X-band EPR study of Gd^{3+}-doped LaF_3, $La_{0.9}Ce_{0.1}F_3$, $La_{0.9}Nd_{0.1}F_3$, $LiYF_4$ and $LiY_{0.9}Yb_{0.1}F_4$ single crystals in the temperature range 4.2–295 K was carried out in order to investigate the Gd^{3+} spin–phonon interactions. Spin-Hamiltonian parameters are analysed in the light of the superposition model and the rotational invariance theory for phonon-induced contributions to spin-Hamiltonian parameters. The $4f^7$ electron–phonon interactions can be described by the Debye model. It is suggested, from the rotational invariance mechanism for phonon-induced contributions to spin-Hamiltonian parameters, that the rotational contributions are much smaller than those from the strain. Temperature-induced distortions of the crystal field, as well as these distortions caused by the La^{3+}/Nd^{3+} and Y^{3+}/Yb^{3+} substitutions, influence significantly the $4f^7$ electron–phonon interactions. The coupling constant K_2 of $4f^7$ electrons to the whole phonon spectrum of the crystal lattice is stronger in the LaF_3, $La_{0.9}Ce_{0.1}F_3$, $La_{0.9}Nd_{0.1}F_3$ with larger temperature-induced distortion of the Gd^{3+} site symmetry than in $LiYF_4$, $LiY_{0.9}Yb_{0.1}F_4$. Our results are compared with those for Gd^{3+}-doped $RbCdF_3$ and PbF_2 single crystals.

PACS numbers: 63.20.Kr, 76.30.Kg

1. Introduction

The LaF_3 and $LiYF_4$ single crystals are the most used fluoride laser host materials, neutron scintillation detectors and radiation hard scintillators for calorimetry at future colliders [1–4]. The X-band (≈ 9.5 GHz) electron paramagnetic resonance (EPR) studies of Gd^{3+}-doped LaF_3, CeF_3, PrF_3, NdF_3, $LiYF_4$, and $LiYbF_4$ single crystals were reported in Refs. [5–7]. A detailed X-band EPR studies were

*corresponding author; e-mail: mlpar@tytan.umcs.lublin.pl

performed in Gd^{3+}-doped $La_xRE_{1-x}F_3$ (RE = Ce, Pr, Nd) and $LiY_{1-x}Yb_xF_4$ single crystals for various values of x and at variable temperatures, in the range 4.2–295 K, in order to investigate crystal field effects [8–13]. The small distortion from the D_{3d}^4 trigonal space group was observed in $La_xCe_{1-x}F_3$ and $La_xNd_{1-x}F_3$ single crystals using magnetic susceptibility method [14, 15]. A small change of the crystal field in LaF_3, $La_{0.9}Ce_{0.1}F_3$, and $La_{0.9}Nd_{0.1}F_3$ with lowering temperature below 150 K, as a result of temperature induced distortion of the crystal lattice was observed in our recent work [11].

The purpose of the present paper is to study the influence of the crystal field distortion on the Gd^{3+} spin–phonon interactions at different temperatures using EPR technique and superposition model, because they are very sensitive to the distortion of the crystal lattice. We have chosen the LaF_3 and $LiYF_4$ to compare how different crystal field symmetries are changed with the temperature. The Debye temperatures of the investigated crystals are comparable. Thus, we can compare the lattice dynamics of LaF_3 and $LiYF_4$ crystals. We have adopted the theory of rotational invariance for phonon-induced contributions to spin-Hamiltonian parameters (SHP) developed by Bates and Szymczak [16, 17], which gives more precise description of the observed contribution to SHP from lattice dynamics. The previous results of temperature EPR (X-band) studies in Gd^{3+}-doped LaF_3, $La_{0.9}Ce_{0.1}F_3$, $La_{0.9}Nd_{0.1}F_3$, $LiYF_4$, and $LiY_{0.9}Yb_{0.1}F_4$ single crystals have been used to investigate influence of structural and crystal field effects on spin–phonon interactions between Gd^{3+} and crystal lattice. The above samples are the only crystals studied in details for which well-resolved EPR spectra can be recorded down to liquid-helium temperature.

2. Crystal structure

The $La_xRE_{1-x}F_3$ (RE = Ce, Nd) and $LiY_{1-x}Yb_xF_4$ ($x = 0{-}1$) single crystals doped with Gd^{3+} (0.1 mol%) were grown from the melt by a modified Bridgman–Stockbarger method [9, 18, 19]. They were transparent and the $La_xRE_{1-x}F_3$ cleft easily in the cleavage planes (001) and (110). The LaF_3, CeF_3, and NdF_3 single crystals have a tysonite structure with the trigonal space-group classification $P\bar{3}c1$ (D_{3d}^4 trigonal symmetry with a hexamolecular unit cell) [9, 18]. The site symmetry of the La^{3+}, Ce^{3+}, and Nd^{3+} ions is C_2. The crystallographic c axis is parallel to the C_3 axis, and perpendicular to the three C_2 axes. There are six molecules per unit cell. The $LiYF_4$ and $LiYbF_4$ crystals have the scheelite ($CaWO_4$) structure with the space-group classification $I4_1/a$ (C_{4h}^6) and the S_4 local symmetry at Y^{3+} or Yb^{3+} sites [19]. They possess a body-centered-tetragonal crystal structure containing four molecules per unit cell. It is assumed that $La_xRE_{1-x}F_3$ single crystals have the tysonite structure, with the a and c dimensions scaled in proportion to x between limit values of lattice constants in LaF_3, CeF_3, and NdF_3. Further, the $LiY_{1-x}Yb_xF_4$ crystals have the scheelite structure with a and c also scaled between lattice constants of $LiYF_4$ and $LiYbF_4$ [12].

3. Results and discussion

The experimental arrangement has been described elsewhere [12]. EPR spectra of the Gd^{3+}-doped LaF_3, $La_{0.9}Ce_{0.1}F_3$, $La_{0.9}Nd_{0.1}F_3$, $LiYF_4$, and $LiY_{0.9}Yb_{0.1}F_4$ single crystals were recorded with the external magnetic field $\boldsymbol{B}$ rotated in the ZX plane at temperatures 4 K $< T <$ 300 K. The ZX plane is the crystallographic (001) plane in $La_xRE_{1-x}F_3$ (RE = Ce, Nd) and (100) plane in $LiY_{1-x}Yb_xF_4$ ($x = 0$–1). The $\boldsymbol{Z}$ ($||\boldsymbol{a}$) axis, along which the overall splitting of EPR lines has a maximum, lies in the plane (001) in $La_xRE_{1-x}F_3$ (RE = Ce, Nd) [11] and the $\boldsymbol{Z}$ ($||\boldsymbol{c}$) axis lies in the (100) plane in $LiY_{1-x}Yb_xF_4$ [12].

The angular variation for Gd^{3+}-doped above single crystals in the ZX plane was shown in Refs. [8, 10, 12, 13]. EPR spectra are consistent with the rhombic C_{2v} site symmetry for the Gd^{3+} ion in the D_{3d}^4 trigonal symmetry of lanthanum fluorides, and the tetragonal D_{2d} site symmetry of lithium–yttrium fluorides. The determined SHP (b_l^m) of Gd^{3+} in $La_xRE_{1-x}F_3$ (RE = Ce, Nd) and $LiY_{1-x}Yb_xF_4$ hosts were fitted successfully in the temperature range 4.2–295 K to the quadratic function [10–13], which suggested the existence of the Gd^{3+} spin–phonon interactions. In order to separate the spin–phonon contribution from that of the thermal expansion we used the superposition model. In this model b_l^m are expressed as linear superpositions of single-ligand contributions to the intrinsic parameters $\bar{b}_l(R_0)$ [20, 21].

We consider the nine nearest neighbour F^- ions to a Gd^{3+} ion substituting for La^{3+}, Ce^{3+}, or Nd^{3+} ion in LaF_3, $La_{0.9}Ce_{0.1}F_3$ and $La_{0.9}Nd_{0.1}F_3$ [9–11]. In the same way, for the $LiYF_4$ and $LiY_{0.9}Yb_{0.1}F_4$, we consider the eight nearest neighbour F^- ions to a Gd^{3+} ion substituting for Y^{3+}, or Yb^{3+} ion [12, 13]. In order to evaluate the intrinsic parameters $\bar{b}_l(R_0)$, the required lattice constants of $La_{0.9}Ce_{0.1}F_3$, $La_{0.9}Nd_{0.1}F_3$, and $LiY_{0.9}Yb_{0.1}F_4$ were estimated using Vegard's law. The unit cell parameters of LaF_3, CeF_3, NdF_3, $LiYF_4$, and $LiYbF_4$ were measured in the range 87–295 K [18, 19]; those parameters at lower temperatures were obtained by extrapolation. The application of the superposition model requires exact knowledge of t_l intrinsic exponential parameters and positions of ligands around the paramagnetic ion. We assumed that $t_2 = 9$ and $t_4 = 14$, which are the same as those for LaF_3, CeF_3, and NdF_3 hosts [6]. In the same way, for $LiYF_4$ and $LiY_{0.9}Yb_{0.1}F_4$ we assumed that $t_2 = 1$ [12, 13]. The major part of the temperature dependence of b_2^0 is due to the spin–phonon interaction effects. Using the data of lattice constants dependent on temperature [18, 19] we evaluate to 33% (in lanthanum fluorides) [10] and 22% (in lithium–yttrium fluorides) [12] the contributions of thermal expansion to the b_2^0 change with temperature. The remaining part (67% for LaF_3 and 78% for lithium–yttrium fluorides) of the b_2^0 change with temperature is due to the modulation of the crystal field by thermally excited phonons. The temperature dependence of b_2^0 is sufficiently reflected by the change of the intrinsic parameter $\bar{b}_2$, because the effect of thermal expansion (contraction) of the lattice on $\bar{b}_2$ is calculated to be rather small.

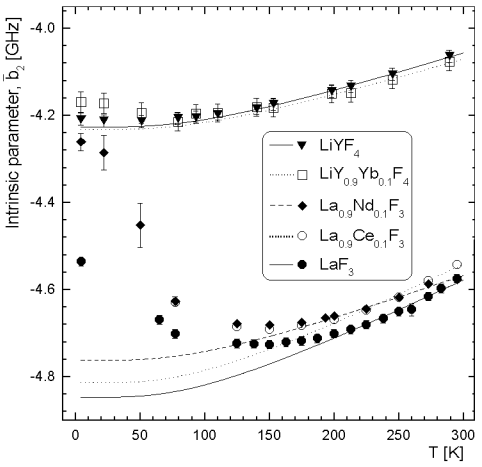

Fig. 1. Temperature dependence of the intrinsic parameter $\bar{b}_2$ for Gd^{3+}-doped LaF_3, $La_{0.9}Ce_{0.1}F_3$, $La_{0.9}Nd_{0.1}F_3$, $LiYF_4$, and $LiY_{0.9}Yb_{0.1}F_4$ single crystals. The curve lines shown here are the best fitted in the temperature ranges 200–295 K for LaF_3, $La_{0.9}Ce_{0.1}F_3$, $La_{0.9}Nd_{0.1}F_3$, and 150–289 K for $LiYF_4$, $LiY_{0.9}Yb_{0.1}F_4$ using Eq. (1). The lines are extrapolated to liquid-helium temperatures at constant parameters K_2 and $\bar{b}_2(\mathrm{RL})$ taken from Table.

Below we consider the successful use of intrinsic parameters to describe the spin–phonon interactions in rare-earth fluorides, since they better represent the crystal field than the parameters b_l^m. The intrinsic parameters $\bar{b}_l$ represent an assemblage of single-particle effects of shielded electrostatic contribution, covalency, overlap and configuration interaction. The ground configuration $4f^7$ is shielded by the $5s^25p^6$ shell of Gd^{3+}, and it causes weaker interaction with ligand ions (F^-) having outer $2s^22p^6$ shell. In practice, we consider only the $\bar{b}_2$ parameter, because it is thought to contain considerable electrostatic contributions from ligands, whereas the $\bar{b}_4$ and $\bar{b}_6$ parameters represent mostly overlap and covalency effects. Experimental data show that the fourth rank SHP are not varied within experimental errors in the temperature range 4.2–295 K for $La_xRE_{1-x}F_3$, whereas for $LiY_{1-x}Yb_xF_4$ are varied very slightly [10, 12, 13]. There is no temperature dependence for the sixth rank SHP in the above single crystals. Thus, from the temperature dependence of $\bar{b}_2$ we can see spin–phonon interactions, since this parameter is very sensitive to the temperature-induced distortion of the crystal field. In order to describe the temperature dependence of $\bar{b}_2$ plotted in Fig. 1 we used the Debye model, which assumes that paramagnetic ions Gd^{3+} are coupled to the whole phonon spectrum of the crystal lattice. The equation adopted to fit $\bar{b}_2$ to temperature T is the following [22]:

$$\bar{b}_2(T) = \bar{b}_2(\mathrm{RL}) + K_2\left(1 + 8\frac{T^4}{\theta_\mathrm{D}^4}\int_0^{\theta_\mathrm{D}/T}\frac{x^3}{\mathrm{e}^x - 1}\mathrm{d}x\right), \qquad (1)$$

where $\bar{b}_2$(RL) is a "rigid lattice" value of $\bar{b}_2$ (i.e. the value of $\bar{b}_2$ at $T = 0$ K minus zero point vibrations), K_2 is the coupling constant describing the magnitude of Gd^{3+} spin–phonon interaction and θ_D is the Debye temperature. The $\bar{b}_2$(RL) and K_2 were determined by fitting the $\bar{b}_2$ from Eq. (1) to our data by the least squares method. We obtained the best fits in the temperature range 200–295 K ($\theta_D = 391$ K [23]) for LaF_3, $La_{0.9}Ce_{0.1}F_3$, $La_{0.9}Nd_{0.1}F_3$, as well as in the range 150–289 K ($\theta_D = 405$ K [24]) for $LiYF_4$ and $LiY_{0.9}Yb_{0.1}F_4$. The results of fittings are given in Table. The $\bar{b}_2$(RL) "rigid lattice" value decreases with increasing mass of rare-earth ions in the lanthanum (rare-earth) fluorides, as well as these values are larger than those in lithium–yttrium (ytterbium) fluorides. The Gd^{3+} spin–phonon interaction coupling constant K_2 is smaller in mixed crystals due to larger dynamic deformation arisen from the substitution of heavier Nd^{3+} and Yb^{3+} for La^{3+} and Y^{3+}, respectively. This coupling constant is larger in LaF_3 than in $LiYF_4$.

The theory of rotational invariance for the phonon-induced contributions to SHP for orbital singlet ions, gives more precise description of the observed contribution to the b_2^0 from lattice dynamics [16, 17]. It is usually difficult to determine magnetoelastic tensor components in low symmetry crystal field, e.g., in LaF_3 and $LiYF_4$ crystals. In order to explain experimentally measured b_2^0 by the above mechanism, we need to separate the thermal expansion from those of the spin–phonon contributions. The spin–phonon contributions are calculated using the $\bar{b}_2$ values, as follows:

$$\delta D = p[\bar{b}_2(T) - \bar{b}_2(\mathrm{RL})], \tag{2}$$

where $p = 0.67$ for $La_xRE_{1-x}F_3$ and $p = 0.78$ for $LiY_{1-x}Yb_xF_4$ in the investigated temperature range 4.2–295 K. The most important contributions to the b_2^0 are due to the lattice anharmonicity. There are two important phonon-induced contributions to b_2^0 — from the strain and from the rotation. The former is responsible for the vibrational modes resulting in the vibration-type displacements of the ligand ions, whereas the latter is responsible for the rotational modes, resulting in the rotation-type displacements of the ligands around the paramagnetic Gd^{3+} ion. In the theory of the magnetoelastic tensor, which is used to describe the interaction between phonons and the spin system, spins are coupled to the lattice via deformations of the lattice expressed by a symmetric, finite elastic strain tensor, and by antisymmetric parts of the strain tensor. Further, the anharmonic contributions from the strain δD and from the rotation δD_r to D ($= b_2^0$) are given by the equations [17]:

$$\delta D = \frac{-\hbar}{32\pi^2\rho}(G_{11} + G_{12} + G_{13})(v_l^{-5} + 2v_t^{-5})f(\omega_D, T), \tag{3}$$

and

$$\delta D_r = \frac{-\hbar}{32\pi^2\rho} D v_t^{-5} f(\omega_D, T), \tag{4}$$

TABLE

Values of the parameters $\bar{b}_2$(RL) and K_2 obtained by a least squares fit of the intrinsic parameters with Eq. (1) in the temperature range 200–295 K (θ_D = 391 K) for Gd^{3+}-doped lanthanum (rare-earth) fluorides, as well as in the range 150–289 K (θ_D = 405 K) for lithium–yttrium (rare-earth) fluorides. The D is the static b_2^0 parameter, and R_0 is the equilibrium reference distance between Gd^{3+} and F^- ions at room temperature. Values of the lattice dynamic parameters δD, δD_r, G, $|\mathcal{R}_D|$, η, and u for the Gd^{3+}-doped crystals at room temperature are determined from Eqs. (2)–(9).

Crystal	LaF_3	$La_{0.9}Ce_{0.1}F_3$	$La_{0.9}Nd_{0.1}F_3$	$LiYF_4$	$LiY_{0.9}Yb_{0.1}F_4$
$\bar{b}_2$(RL)	−5.0691	−5.0394	−4.9244	−4.3744	−4.3730
[GHz]	(100)	(121)	(114)	(137)	(202)
K_2	0.2219	0.2254	0.1621	0.1480	0.1408
[GHz]	(17)	(19)	(24)	0.1480(1)	0.1408(2)
D	0.7009	0.6991	0.6956	−2.4863	−2.4830
[GHz]	(20)	(20)	(20)	(20)	(125)
δD	0.3316	0.3331	0.2334	0.2425	0.2312
[GHz]	(134)	(148)	(143)	(126)	(318)
	-562.6^a	-563.9^a	-547.0^a	1008.0^a	957^a
δD_r	(1.6)	(1.6)	(1.6)	(0.6)	(5)
[GHz]/10^5	-509.3^b	-510.5^b	-495.2^b	1023.9^b	972^b
	(1.5)	(1.5)	(1.4)	(0.6)	(5)
	-20.53^a	-20.52^a	-14.75^a	-29.37^a	-29.47^a
G	(0.83)	(0.91)	(0.91)	(1.53)	(4.05)
[GHz]	-22.56^b	-22.55^b	-16.21^b	-28.50^b	-28.59^b
	(0.91)	(1.00)	(1.00)	(1.48)	(3.93)
	16.97^a	16.93^a	23.44^a	41.57^a	41.39^a
$\lvert\mathcal{R}_D\rvert$	(0.73)	(0.80)	(1.51)	(2.18)	(5.89)
$\times 10^{-3}$	15.36^b	15.33^b	21.22^b	42.23^b	42.04^b
	(0.66)	(0.73)	(1.36)	(2.22)	(5.99)
	16.15^a	16.23^a	15.82^a	8.25^a	7.85^a
η	(1.31)	(1.44)	(1.94)	(0.86)	(2.16)
$\times 10^{-3}$	14.70^b	14.77^b	14.40^b	8.51^b	8.09^b
	(1.19)	(1.31)	(1.77)	(0.88)	(2.22)
R_0	2.4187	2.4168	2.4133	2.2695	2.2669
[Å]	2.4187	2.4168	2.4133	2.2695	2.2669
	0.3074^a	0.3079^a	0.3036^a	0.2062^a	0.2008^a
u	(124)	(137)	(187)	(107)	(279)
[Å]	0.2932^b	0.2937^b	0.2896^b	0.2093^b	0.2039^b
	(119)	(131)	(178)	(109)	(283)

[a]determined for elastic waves polarized in the [001] direction; [b]determined for elastic waves polarized in the [100] and [010] directions

where G_{11}, G_{12}, G_{13} are the components of the A_1-type magnetoelastic tensor (fully symmetric deformation), ρ is the crystal density, v_l and v_t are the longitudinal and the transversal velocities of sound, respectively, and

$$f(\omega_{\mathrm{D}}, T) = \omega_{\mathrm{D}}^4 + 8\left(\frac{kT}{\hbar}\right)^4 \int_0^{\theta_{\mathrm{D}}/T} \frac{x^3}{\mathrm{e}^x - 1}\mathrm{d}x \tag{5}$$

with $\hbar\omega_{\mathrm{D}} = k\theta_{\mathrm{D}}$.

The values of sound velocities at room temperature are taken from Refs. [23, 25, 26] for the elastic waves polarized in the [100], [010] and [001] directions. We calculated those sound velocities at lower temperatures using elastic constants [25, 26]. The ratio of the anharmonic contributions from the rotation to contributions from the strain is given by the relation [17]:

$$\mathcal{R}_{\mathrm{D}} = \frac{\delta D_{\mathrm{r}}}{\delta D}. \tag{6}$$

The calculations from Eqs. (2)–(6) yield the values of anharmonic contributions from the strain δD and from the rotation δD_{r}, the sum values of magnetoelastic tensor components $G = G_{11} + G_{12} + G_{13}$ and the ratio $\mathcal{R}_{\mathrm{D}}$ (Table). The results of the ratio $\mathcal{R}_{\mathrm{D}}$ for the investigated samples at room temperature are in agreement with those of obtained in Ref. [17], using the isotropic continuum phonon model for orbital singlet ions in low symmetry crystal field; i.e. the rotational contributions are much smaller than those from the strain.

The Gd^{3+} spin–phonon interaction constant K_2 given in Eq. (1) can be expressed in terms of the magnetoelastic tensor components as follows:

$$K_2 = \frac{-\hbar\omega_{\mathrm{D}}^4(v_l^{-5} + 2v_t^{-5})}{32p\pi^2\rho}(G_{11} + G_{12} + G_{13}). \tag{7}$$

The parameter η describing the strength of the dynamical part of the crystal field can be evaluated from the formula

$$\eta = \frac{\delta D}{|G|}. \tag{8}$$

On the other hand, the parameter η is defined by the expression [27]:

$$\eta = \frac{\langle u^2 \rangle}{R_0^2}, \tag{9}$$

where $\langle u^2 \rangle$ is the mean square displacement of the ligands from their equilibrium positions, and R_0 is the equilibrium minimal distance between the rare-earth ion and the ligands.

The determined from Eqs. (8) and (9) values of the parameter η and the amplitude u of vibrations of ligands in the investigated samples at room temperature are given in Table. It can be seen that the values of the dynamical parameters G, $\mathcal{R}_{\mathrm{D}}$, η and u determined for the elastic waves polarized in the [001], [100] and [010] directions are equal each to each within the errors. The values

of the dynamical parameter δD_{r} differ slightly in these directions due to small anisotropy of transversal sound velocity. It confirms correctness of using the rotational invariance theory for the phonon-induced contributions to SHP for orbital singlet ions in low symmetry crystal fields. The temperature dependence of G, determined from Eqs. (2), (3) and (5), is plotted in Fig. 2. There is a significant variation of G with temperature for LaF_3, whereas for $LiYF_4$ this parameter is varying very slightly. Determined from Eqs. (7) and (8) the Gd^{3+} spin–phonon interaction coupling constant K_2 and the parameter η are plotted in Figs. 3 and 4, respectively. It can be seen that values of these parameters for Gd^{3+}-doped LaF_3 are changed stronger with temperature than those for $LiYF_4$. It suggests that the static distortion of the Gd^{3+} site symmetry increases with decreasing temperature in the former crystal. In addition, we have plotted the absolute values of the ratio $|\mathcal{R}_{\mathrm{D}}|$ in Fig. 5. The ratio $|\mathcal{R}_{\mathrm{D}}|$ is larger approximately by factor 3 in $LiYF_4$, $LiY_{0.9}Yb_{0.1}F_4$ and by factor 1.5 in $La_{0.9}Nd_{0.1}F_3$ than in LaF_3 and $La_{0.9}Ce_{0.1}F_3$ (Table). On the other hand, the Gd^{3+} spin–phonon interaction coupling constant K_2 is smaller in crystals with larger rotational contributions, showing that vibrational modes are coupled stronger to spins than rotational modes. Further, the temperature dependence of K_2 is reflected by decrease in the η

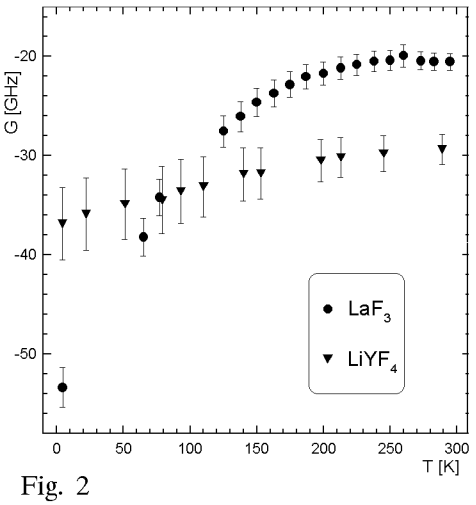

Fig. 2

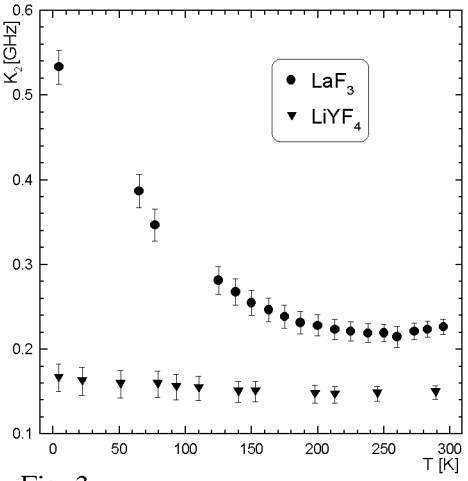

Fig. 3

Fig. 2. Temperature dependence of the sum values of magnetoelastic tensor components $G = G_{11} + G_{12} + G_{13}$ for elastic waves polarized in the [001] direction for Gd^{3+}-doped LaF_3 and $LiYF_4$ single crystals.

Fig. 3. Temperature dependence of the $4f^7$ electron–phonon coupling constant K_2 for elastic waves polarized in the [001] direction for Gd^{3+}-doped LaF_3 and $LiYF_4$ single crystals.

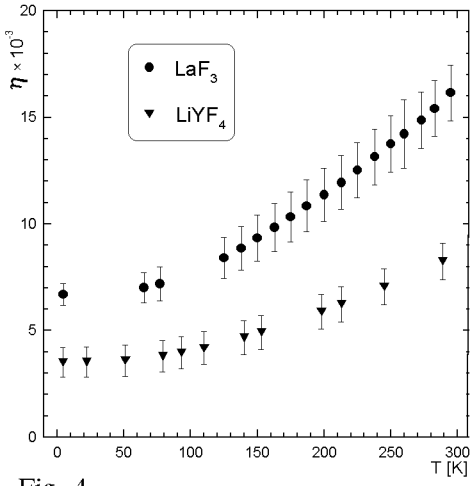

Fig. 4

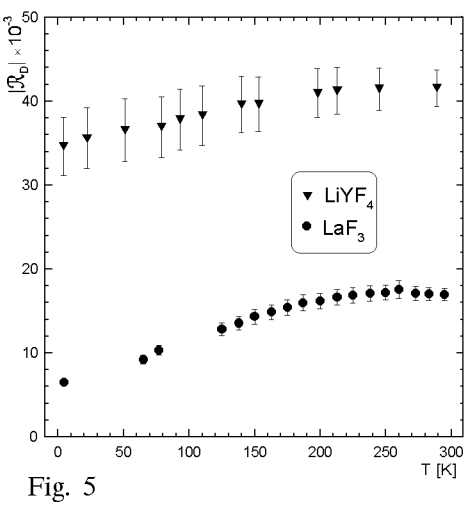

Fig. 5

Fig. 4. Temperature dependence of the parameter η from vibration-type displacements in the [001] direction of the ligand F^- ions for Gd^{3+}-doped LaF_3 and $LiYF_4$ single crystals.

Fig. 5. Temperature dependence of the absolute value of the ratio $|\mathcal{R}_D|$ of the anharmonic rotational to the vibrational contributions for Gd^{3+}-doped LaF_3 and $LiYF_4$ single crystals.

and the $|\mathcal{R}_D|$ values with temperature (Figs. 3, 4, and 5). The coupling constant K_2 between $4f^7$ electrons and phonons in LaF_3 is about 1.5, 2.2, and 3.2 times larger than in $LiYF_4$ at room, liquid-nitrogen and liquid-helium temperatures, respectively. This statement can be confirmed by optical measurements at 77 K, implying the larger amplitude u of the lattice zero vibrations and parameter η in LaF_3 ($u = 4.69\times10^{-2}$ Å and $\eta = 3.64\times10^{-4}$) versus $LiYF_4$ ($u = 3.77\times10^{-2}$ Å and $\eta = 2.35\times10^{-4}$) [27]. The ratio of $\eta(LaF_3)/\eta(LiYF_4)$ gives 1.55 in Ref. [27] which is close to 1.89 ± 0.58 in this paper at 77 K. Further, for comparison we have determined $u = 20.47\times10^{-2}$ Å in LaF_3 and $u = 13.95\times10^{-2}$ Å in $LiYF_4$. Orlovskii et al. [27] used the point-charge nonlinear relaxation theory, assuming a harmonic approximation for the crystal lattice vibrations and determined one order of magnitude smaller values of η and about 4 times smaller u than EPR technique due to considering higher-lying excited multiplets of Nd^{3+}, between which transitions produce mainly optical phonons. Further, the same order of magnitude of amplitude u as in present paper is determined from a model of the transferred hyperfine interaction of ^{19}F ligands with Gd^{3+} in PbF_2 [28].

The coupling of the $4f^7$ electrons to the whole phonon spectrum stronger than in our crystals exists in the Gd^{3+}-doped $RbCdF_3$ single crystal, due to the dynamics of charge compensators causing a tetragonal distortion of the crystal field. The value of $K_2 = -0.7735(24)$ GHz for Gd^{3+}-doped $RbCdF_3$ was determined

from the temperature dependence of b_2^0 [22], as compared to $K_2 = 0.2219(17)$ GHz for LaF_3 or $K_2 = 0.1480(1)$ GHz for $LiYF_4$. On the other hand, in Gd^{3+}-doped PbF_2 single crystal the value of $K_2 = -0.1079$ GHz for tetragonal deformations and $K_2 = 0.3688$ GHz for trigonal deformations was obtained from EPR uniaxial stress experiment in the temperature range 130–600 K by Kuriata et al. [29]. This shows that distortion of the crystal field (trigonal is lower symmetry than tetragonal) influences significantly the $4f^7$ electron–phonon coupling constant K_2. These results from the literature support our data, since they are of the same order of magnitude. It argues existence of a mechanism responsible for the Gd^{3+} spin–phonon interactions, which is caused by the distortion of the Gd^{3+} site symmetry.

A mechanism responsible for the $4f^7$ electron–phonon interaction may be also related partly to the polarization of ligand F^- ions. The polarizability depends on the surroundings of the F^- ion, and it is larger in $LiYF_4$ than in LaF_3. Electrostatic polarization of the ligands, caused by distortion of the lattice, can produce a large contribution to the $\bar{b}_2$. The lattice dynamics due to the strain (δD) and due to the rotational-type displacements of the ligand F^- ions (δD_{r}), as well as the temperature-induced distortion of a Gd^{3+} site symmetry influence significantly the charge distribution of the $4f^7$ shell. The temperature-induced distortion of the Gd^{3+} site symmetry and the parameter η are larger, and on the other hand, the parameter $|\mathcal{R}_{\mathrm{D}}|$ is smaller in LaF_3 than in $LiYF_4$. These static and dynamic effects can cause that the $4f^7$ electrons are more spherically distributed in $LiYF_4$ than in LaF_3. In addition, the lowering of a Gd^{3+} site symmetry with temperature causes an increase in a number of low-frequency vibrational modes, as it is known from theory of groups. Such mechanism explains strong coupling of the Gd^{3+} ions with vibrations of the crystal lattice in LaF_3 than in $LiYF_4$. It is confirmed by determined higher frequency of phonon spectrum in $LiYF_4$ [30, 31], as compared to lower frequency phonons in LaF_3 [32]. Salaün et al. [30, 31] performed Raman, infrared and inelastic neutron scattering study of the $LiYF_4$ and of $LiLnF_4$ series of compounds (Ln = Ho, Er, Tm, Yb; Y). They report that the heavy Ln ions are not involved in the lowest frequency optical A_{u} and E_{u} modes. It was deduced that only Raman-active modes at low frequencies with E_{g} and B_{g} symmetries can imply lanthanide vibrations in the (001) plane and along the [001] direction, respectively. A combination of Y^{3+} translation in the (001) plane, plus the rotation around the a-axis of fluorine ions causes an angular distortion. Thus, the five symmetric and the four antisymmetric modes were found for vibrations of fluorine ions [31]. It supports the larger rotation-type displacements of the F^- ions in $LiYF_4$ and $LiY_{0.9}Yb_{0.1}F_4$ crystals, contrary to LaF_3, $La_{0.9}Ce_{0.1}F_3$, and $La_{0.9}Nd_{0.1}F_3$ crystals.

4. Conclusions

It is concluded that the $4f^7$ electron–phonon interactions are strongly dependent on the local structure deformation of the site symmetry of Gd^{3+} ion. Although the variation of the distortion of the local site symmetry is small, it has a drastic effect on the constant K_2, which describes the coupling between $4f^7$ electrons and whole phonon spectrum of the crystal lattice. The temperature dependence of K_2 is stronger in LaF_3 than in $LiYF_4$ due to the larger temperature-induced distortion of Gd^{3+} site symmetry in LaF_3, contrary to $LiYF_4$. The lattice dynamics parameters η and $\mathcal{R}_D$ influence significantly the $4f^7$ electron–phonon coupling constant K_2 in the investigated crystals. Further, the values of $\mathcal{R}_D$ in these crystals show that the rotational contributions to the Gd^{3+} SHP from phonons are much smaller than those from the strain. In the present paper we show the successful way to study the lattice dynamics (from ligands) using the EPR technique and the superposition model, as well as the rotational invariance theory for phonon-induced contributions to SHP from lattice anharmonicity.

References

[1] A.A. Kaminskii, H.R. Verdun, *Phys. Status Solidi A* **129,** K119 (1992).

[2] P. Dorenbos, J.T.M. De Haas, C.W.E. Van Eijk, *J. Lumin.* **69,** 229 (1996).

[3] A.R. Spowart, *J. Phys. D* **16,** 1819 (1983).

[4] E. Auffray, S. Baccaro, T. Beckers, Y. Benhammou, A.N. Belsky, B. Borgia, D. Boutet, R. Chipaux, I. Dafinei, F. de Notaristefani, P. Depasse, C. Dujardin, H. El Mamouni, J.L. Faure, J. Fay, M. Goyot, S.K. Gupta, A. Gurtu, H. Hillemanns, B. Ille, T. Kirn, M. Lebeau, P. Lebrun, P. Lecoq, J.A. Mares, J.P. Martin, V.V. Mikhailin, B. Moine, J. Nelissen, M. Nikl, C. Pedrini, R. Raghavan, P. Sahuc, D. Schmitz, M. Schneegans, J. Schwenke, S. Tavernier, V. Topa, A.N. Vasil'ev, M. Vivargent, J.P. Walder, *Nucl. Instrum. Methods Phys. Res. A* **383,** 367 (1996).

[5] S.K. Misra, P. Mikołajczak, S. Korczak, *J. Chem. Phys.* **74,** 922 (1981).

[6] S.K. Misra, P. Mikołajczak, N.R. Lewis, *Phys. Rev. B* **24,** 3729 (1981).

[7] S.K. Misra, M. Kahrizi, P. Mikołajczak, L.E. Misiak, *Phys. Rev. B* **32,** 4738 (1985).

[8] M.L. Paradowski, L.E. Misiak, *Nukleonika* **42,** 543 (1997).

[9] M.L. Paradowski, W. Korczak, L.E. Misiak, Z. Korczak, *Proc. SPIE* **3724,** 47 (1999).

[10] M.L. Paradowski, L.E. Misiak, *Acta Phys. Pol. A* **95,** 367 (1999).

[11] M.L. Paradowski, L.E. Misiak, W. Korczak, Z. Korczak, *Proc. SPIE* **4412,** 242 (2001).

[12] L.E. Misiak, S.K. Misra, P. Mikołajczak, *Phys. Rev. B* **38,** 8673 (1988).

[13] L.E. Misiak, P. Mikołajczak, *Acta Phys. Pol. A* **75,** 621 (1989).

[14] M.L. Paradowski, A. Pacyna, A. Bombik, W. Korczak, S.Z. Korczak, *J. Magn. Magn. Mater.* **166,** 231 (1997).

[15] M.L. Paradowski, A. Pacyna, A. Bombik, W. Korczak, S.Z. Korczak, *J. Magn. Magn. Mater.* **212,** 381 (2000).

[16] C.A. Bates, H. Szymczak, *Phys. Status Solidi B* **74,** 225 (1976).

[17] C.A. Bates, H. Szymczak, *Z. Phys. B* **28,** 67 (1977).

[18] W. Korczak, P. Mikołajczak, *J. Cryst. Growth* **61,** 601 (1983).

[19] L.E. Misiak, P. Mikołajczak, M. Subotowicz, *Phys. Status. Solidi A* **97,** 353 (1986).

[20] D.J. Newman, W. Urban, *J. Phys. C* **5,** 3101 (1972).

[21] D.J. Newman, W. Urban, *Adv. Phys.* **24,** 793 (1975).

[22] N. Guskos, J. Kuriata, T. Rewaj, *Acta Phys. Pol. A* **81,** 659 (1992).

[23] A.E. Aliev, V.F. Krivorotov, P.K. Khabibullaev, *Fiz. Tverd. Tela* **39,** 1548 (1997).

[24] L.E. Misiak, M. Subotowicz, *Solid State Commun.* **80,** 761 (1991).

[25] R. Laiho, M. Lakkisto, T. Levola, *Philos. Mag. A* **47,** 235 (1983).

[26] P. Blanchfield, G.A. Saunders, *J. Phys. C, Solid State Phys.* **12,** 4673 (1979).

[27] Y.V. Orlovskii, R.J. Reeves, R.C. Powell, T.T. Basiev, K.K. Pukhov, *Phys. Rev. B* **49,** 3821 (1994).

[28] J.M. Baker, *J. Phys. C, Solid State Phys.* **12,** 4039 (1979).

[29] J. Kuriata, T. Rewaj, N. Guskos, *Acta Phys. Pol. A* **79,** 531 (1991).

[30] S. Salaün, M.T. Fornoni, A. Bulou, M. Rousseau, P. Simon, J.Y. Gesland, *J. Phys., Condens. Matter* **9,** 6941 (1997).

[31] S. Salaün, A. Bulou, M. Rousseau, B. Hennion, J.Y. Gesland, *J. Phys., Condens. Matter* **9,** 6957 (1997).

[32] R.S. Meltzer, J.E. Rives, G.S. Dixon, *Phys. Rev. B* **28,** 4786 (1983).